

Quantum Monte Carlo study of the Protonated Water Dimer

Mario Dagrada,^{1,*} Michele Casula,^{1,†} Antonino M. Saitta,^{1,‡} Sandro Sorella,^{2,§} and Francesco Mauri^{1,¶}

¹*CNRS and Institut de Minéralogie et de Physique des Milieux condensés,
Université Pierre et Marie Curie, case 115, 4 place Jussieu, 75252, Paris cedex 05, France*

²*International School for Advanced Studies (SISSA) Via Beirut 2,4 34014 Trieste,
Italy and INFN Democritos National Simulation Center, Trieste, Italy*

(Dated: January 8, 2022)

We report an extensive theoretical study of the protonated water dimer $H_5O_2^+$ (Zundel ion) by means of the highly correlated variational Monte Carlo and lattice regularized Monte Carlo approaches. This system represents the simplest model for proton transfer (PT) and a correct description of its properties is essential in order to understand the PT mechanism in more complex aqueous systems. Our Jastrow correlated AGP wave function ensures an accurate treatment of electron correlations. Exploiting the advantages of contracting the primitive basis set over atomic hybrid orbitals, we are able to limit dramatically the number of variational parameters with a systematic control on the numerical precision, a crucial ingredient in order to simulate larger systems. We investigate the energetics and geometrical properties of the $H_5O_2^+$ as a function of the oxygen-oxygen distance, taken as reaction coordinate. In both cases, our QMC results are found in excellent agreement with state-of-the-art coupled cluster CCSD(T) techniques. Calculations on proton transfer static barriers and dissociation energies display the same agreement. A comparison with density functional theory results in the PBE approximation points out the crucial role of electron correlations for a correct description of the PT in the dimer. Finally, the ability of our method to resolve very tiny energy differences (~ 0.1 Kcal/mol) at which the proton hopping takes place and the corresponding structural variations optimized directly in the VMC framework is also proven. Our approach combines these features with a N^3 - N^4 scaling with number of particles. This value is favorable with respect to other highly correlated *ab initio* approaches and it allows the simulation of more realistic PT models; a test calculation on a larger protonated water cluster is hence carried out. The QMC approach used here represents a promising candidate to provide the first high-level *ab-initio* description of PT in water.

I. INTRODUCTION

Water is a key element for life, but nevertheless its properties arising from its unique structure are not fully understood yet. A large amount of published works explored the several phases of water and many efforts have been spent by the scientific community in order to match experimental findings with theoretical predictions.

From the chemical and biological points of view, a deep understanding of the properties of aqueous systems and therefore of liquid water is fundamental. Over the past years, the structural and dynamical properties of liquid water have been investigated relying on the state-of-the-art molecular dynamics techniques such as empirical force field methods¹⁻³ and *ab initio* molecular dynamics (AIMD). The latter methodology has been extensively employed for the study of liquid water⁴⁻⁸ as well as aqueous solution of biological interest^{9,10}; within, this technique, the atomic force fields required as input by any molecular dynamics simulation are constructed from *ab initio* potential energy surfaces (PESs) and therefore directly derived from first principles electronic structure calculations.

Working out an accurate PES for liquid water has been a longstanding challenge in the scientific community; this is due mainly to the absence of an *ab initio* method able to develop a reliable PES that describes breaking and formation of hydrogen bonds; other issues are related to difficulties in simulating weak interaction and polariza-

tion effects in the network of polar molecules.

The simulation of liquid systems requires model clusters with a large amount of molecules and therefore a good scalability is fundamental in order to carry out simulations in a reasonable computational time; therefore the technique which has been mostly employed over the past years is density functional theory (DFT) which combines scalability and flexibility features. Nevertheless, molecular dynamics simulations which start from DFT-based PES fail in reproducing basic properties of liquid water such as the melting point temperature¹¹ and the oxygen-oxygen radial distribution function g_{OO} ¹².

Another major problem which has not been elucidated yet by AIMD is the description of proton transfer (PT) in liquid water, phenomenon which goes under the name of Grotthuss mechanism¹³⁻¹⁵. This process is extremely important in a wide range of biological systems and it influences many dynamical processes in material science, biochemistry and bioenergetics; for example, PT is one of the main mechanism for charge transport through the cell membranes^{16,17}; it plays an important role in several enzymatic reactions and photosynthesis^{18,19} and moreover proton has the role of mediator and promoter of many acid-base reactions in solution²⁰⁻²².

Although over the past years many experimental and theoretical works have been devoted to the study of Grotthuss reaction, an accurate quantitative explanation of the underlined mechanism is not fully reached yet. Theoretical investigations still fail in PT basic

properties predictions, such as the activation barrier. Experimental measures of this quantity have been carried out^{23,24} and followed by many attempts of its numerical estimation^{25,26,38}, without a satisfactory accordance. Nevertheless, over the past years AIMD simulations have given many insights on the physics of Grotthuss mechanism^{25,27-31}. It has been found that proton transport is abnormally high and it is not driven by any ordinary diffusion process. The picture which is instead commonly accepted describes the translocation of excess positive charge along the hydrogen-bonded network as structural diffusion of the defects. Ref. 31 has very recently shed new lights on proton transfer and has highlighted the complex nature of the process which involves both structural and dynamical changings of the hydrogen-bonded network.

One of the main issues which sets back from a complete understanding of PT in water, is related to the very sensitive thermal behavior of PT. The required PES precision of the order of few tenths of Kcal/mol has been reached only recently by the state-of-the-art computational methods beyond DFT, such as coupled cluster (CC), multi-reference configuration interaction (MRCI) and the full configuration interaction quantum Monte Carlo (FCIQMC) methods; on the other hand, they are characterized by a much poorer scalability with respect to DFT and therefore they do not allow simulation of sufficiently large molecular clusters.

Over the past years, two main structural models has been proposed to explain proton hydration: M. Eigen³² considered as core of PT the complex $H_9O_4^+$ in which an hydronium H_3O^+ is strongly bounded to three water molecules; G. Zundel³³ proposed a different reaction which involves the simpler $H_5O_2^+$ complex (the “Zundel ion” or “protonated water dimer”) as core of the transfer of proton between two H_2O molecules.

It has been demonstrated²⁷ that these two models occur only as limiting or ideal structures for a more complex phenomenon which involves a large portion of the hydrogen-bonded network. Nevertheless they constitute a perfect testing ground for the most advanced simulation techniques. In particular, the protonated water dimer $H_5O_2^+$ is the smallest system in which an excess proton is shared between water molecules; due to its simplicity, many studies have been carried out to elucidate its properties. Over the past years, several accurate theoretical works have appeared on the Zundel ion to study its structure and energetics³⁴⁻³⁸; the fast development of spectroscopical instruments allowed to probe experimentally vibrational properties of ionic species and therefore many studies on this side have been published⁴⁰ on $H_5O_2^+$. Also molecular dynamics simulations which include quantum effects via Feynman path integrals have been performed (see Ref. 39 as a relevant example) and recently an accurate PES has been produced⁴¹ with state-of-the-art coupled cluster technique including single, double and perturbative triple excitations (CCSD(T)).

In the present paper, we report on an extensive study

of the protonated water dimer using a quantum Monte Carlo (QMC) approach based on a highly correlated variational wave function for energy and geometry calculations. This approach has a very good scalability with the number of particles with respect to other post-DFT methods. We demonstrate that it also insures the precision of a few tenths of Kcal/mol required for an accurate study of the system. These appealing targets are achieved by our Jastrow correlated antisymmetrized geminal power wave function (JAGP), developed on an efficient contracted single particle basis set. While the JAGP provides the necessary ingredients to treat both dynamical and static correlations, the contracted basis set, based on atomic hybrid orbitals, reduces dramatically the computational cost to optimize the JAGP wave function. Thanks to these promising features, we hope that it will pave the way to a complete understanding of the underlined physics of PT and other properties of liquid water.

The paper is organized as follows. In Sec II we introduce the computational techniques used in this work. In particular, in Subsec. II B we describe the variational ansatz and basis set which are the optimal compromise between accuracy and computational cost for water clusters. In Sec. III A we present our results on the single H_2O molecule, the subject of a vast amount of literature. It represents thus the most suitable system for a first benchmark of our approach. For the single H_2O , we study the basis set and wave function convergence and show that we have an accuracy comparable to the latest QMC studies. Sec. III B is devoted to the main results of our paper on the protonated water dimer. We performed structural calculations which aim at finding the ground state geometry of $H_5O_2^+$ at the JAGP level of theory. In order to work out a zero-temperature potential energy landscape, we chose the distance between the two oxygens as a natural reaction coordinate. Along this path, we investigated how the symmetric “Zundel” configuration - namely the one with the proton evenly shared between the two oxygens - evolves to a symmetry-broken geometry, where the excess proton is more bounded to one of the two molecules. We believe that this crossover is critical to understand the physics of PT in larger water clusters. Here we show how our approach describes this relevant region of the $H_5O_2^+$ PES. The evaluation of proton transfer static barriers at fixed \overline{OO} distances shows that our QMC approach has a global accuracy close to the state-of-the-art CCSD(T) calculations performed by Huang et al.⁴¹, with a discrepancy of 0.2 Kcal/mol obtained by diffusion Monte Carlo (DMC) on the variational Monte Carlo (VMC) geometries. In conclusion (Sec. IV), we show that the favorable scalability of our method allows one to simulate larger protonated water clusters in a reasonable computational cost without losing the accuracy reached in the smaller Zundel ion. For the sake of test, we performed a structural optimization on a more realistic PT model, i.e. the cluster of 6 water molecules and one excess proton, to study the behavior of

the computational cost with the system size in practice.

II. COMPUTATIONAL METHODS

A. Density Functional Theory calculations

In this Section we present how we performed DFT-based calculations on the Zundel ion. They are carried out to obtain optimized starting geometries and wave functions for further quantum Monte Carlo calculations.

The DFT geometry has been obtained by a Car-Parrinello dynamics performed in a plane waves basis set with the QUANTUM ESPRESSO⁴² suite of codes. The technical details of this calculation are reported in Subsec. II A 1.

Once the ground-state DFT geometry is found, the Kohn-Sham (KS) orbitals, used as starting input of our QMC wave function, are determined by the DFT code of the TURBORVB package⁴³ which works in a localized Gaussian basis set, as described in Subsec. II A 2.

1. Plane waves DFT

With the aim at finding the optimal DFT geometry for further QMC structural relaxation (see Sec. II B 2), we use the Perdew-Burke-Ernzerhof⁴⁴ (PBE) version of the generalized gradient approximation for the exchange-correlation functional. It has been proven to be quite reliable in describing properties of liquid water⁴⁵. Core electrons are taken into account using a norm conserving Trouiller-Martins pseudopotential⁴⁶. The Kohn-Sham orbitals are expanded over plane waves up to a cutoff of 37.5 H for the wave function and 150 H for the charge density in a periodic box of 30 Bohr radii (a_0) per side.

The zero-temperature geometry relaxation is performed with damped dynamics within the Car-Parrinello (CP) approach⁴⁷. This method allows a very small force convergence threshold of $\sim 10^{-5}$ H/ a_0 on each atomic component at the end of the relaxation. The potential energy surface of the dimer is very flat³⁴ and it develops on energy differences of less than 1 Kcal/mol. Therefore such an accuracy on atomic forces is essential for the minimization to provide a reliable DFT description of the system.

2. Gaussian DFT

We perform gaussian DFT calculations with both pseudopotentials and full electron-ion potentials. The single-particle Kohn-Sham (KS) orbitals $\{\phi_i(\mathbf{r})\}$ are used later on as optimized starting guess for the QMC wave function, as discussed in Sec. II B 1.

The one-body DFT wave function is expanded over a primitive basis of *Gaussian type orbitals* (GTO's) cen-

tered on the atom a , defined up to a normalization constant as:

$$\psi_{a,(l,m,n)}^{\text{GTO}}(\mathbf{r}) \propto |\mathbf{r} - \mathbf{R}_a|^l e^{-\zeta_{l,n}|\mathbf{r} - \mathbf{R}_a|^2} Z_{l,m}(\Omega_{\mathbf{r} - \mathbf{R}_a}), \quad (1)$$

with $m \in [-l, l]$ and $n \in [1, n_l]$, where $\{l, m\}$ are angular momentum quantum numbers, n_l identifies the number of Gaussians for each angular momentum shell, $Z_{l,m}(\Omega)$ are the spherical harmonics, and \mathbf{r} and \mathbf{R}_a are the electron and ion positions, respectively. Our DFT basis set is *even tempered*, namely for each angular momentum l the exponents of the Gaussians are expressed as a power series: $\zeta_{l,n} = \alpha_l \beta_l^{n-1}$ for $n = 1, \dots, n_l$. This allows a reduction of the number of parameters, as for each shell l the full $\zeta_{l,n}$ series is fixed just by three values: α_l , β_l , and n_l . Denoting the set of GTO quantum numbers as $\mu = \{l, m, n\}$, the DFT orbitals $\{\phi_i(\mathbf{r})\}$ expanded over the primitive basis set read:

$$\phi_i(\mathbf{r}) = \sum_a^{N_{\text{atoms}}} \sum_{\mu}^{N_{\text{basis}}(a)} c_{a,\mu}^i \psi_{a,\mu}^{\text{GTO}}(\mathbf{r}), \quad (2)$$

where N_{atoms} identifies the number of atoms of the system, $N_{\text{basis}}(a)$ is the size of the GTO set of the atom a . Thus the global DFT wave function can be expressed as the determinant of the matrix $\{\hat{\phi}_i(\mathbf{x}_j)\}$:

$$\Psi_{\text{DFT}}(\mathbf{x}_1, \dots, \mathbf{x}_N) = \det \hat{\phi}_i(\mathbf{x}_j), \quad (3)$$

with $\{\mathbf{x}_i = (\mathbf{r}_i, \sigma_i)\}$ the spatial and spin coordinates of the N electrons in the system, and $\hat{\phi}_i(\mathbf{x}_j) = \phi_i(\mathbf{r}_j) \sigma_i$ are the spin orbitals.

The ab-initio Hamiltonian of a quantum system is characterized by the divergence of the Coulomb potential at the electron-electron and electron-ion coalescence points. When the potential energy becomes infinite, the wave function of the system must have a cusp to cure the corresponding singularity of the Hamiltonian⁴⁸. These singularities represent a serious issue when an approximated wave function ansatz is employed to solve the Schrödinger equation of a quantum system.

Within a DFT framework, the divergence created by electron-electron coalescence is intrinsically solved by the mean-field description of the system, which maps the interacting Hamiltonian onto a one with independent electrons. Nevertheless, the electron-ion coalescence still represents a problem. One way to cure the latter divergence is to employ a smooth pseudopotential. The pseudo-interaction is chosen such that it eliminates the need of electron-ion cusps in the wave function, by leading to a faster basis set convergence.

In this work we employ an alternative way to solve this issue. We introduce an additional factor to the DFT wave function ansatz which automatically satisfies the electron-ion cusp conditions and cancels out the corresponding divergences of the Hamiltonian.

We rewrite Eq. 3 as:

$$\tilde{\Psi}_{\text{DFT}}(\mathbf{x}_1, \dots, \mathbf{x}_N) = J_1(\mathbf{r}_1, \dots, \mathbf{r}_N) \det \hat{\phi}_i(\mathbf{x}_j), \quad (4)$$

where the function J_1 is called one-body Jastrow factor, borrowed from the QMC notation. It is defined by means of a simple function $u(\mathbf{r})$ which contains only one variational parameter b :

$$u(|\mathbf{r} - \mathbf{R}|) = \frac{1 - e^{-b|\mathbf{r} - \mathbf{R}|}}{2b}. \quad (5)$$

The one-body Jastrow factor J_1 then reads:

$$J_1 = \exp \left(- \sum_i^N \sum_j^{N_{\text{atoms}}} (2Z_j)^{3/4} u((2Z_j)^{1/4} |\mathbf{r}_i - \mathbf{R}_j|) \right), \quad (6)$$

where \mathbf{R}_j are the atomic coordinates corresponding to the atomic number Z_j . In the function u , the multiplicative factor $(2Z_j)^{3/4}$ is set by the electron-ion cusp conditions, while the scaling length $(2Z_j)^{1/4}$ deals with the large distance behavior set by the random phase approximation⁴⁹.

Eq. 4 has the typical functional form of the Jastrow-single determinant (JSD) variational ansatz for quantum Monte Carlo calculations. Indeed the one-body Jastrow of Eq. 6 has been introduced in Ref. 50 to provide a solution of the electron-ion cusp conditions within a QMC framework. Differently from QMC, our $\tilde{\Psi}_{\text{DFT}}$ presents only the one-body Jastrow factor since in DFT the many-body electron-electron interaction is solved within a mean-field description.

By letting the wave function to fulfill the electron-ion cusp conditions, we are able to perform calculations considering the bare interaction for both oxygen and hydrogen atoms (full potential calculations). Furthermore, at variance with conventional DFT calculations based on gaussian localized orbitals, in our approach all the overlap matrix elements involved are computed as numerical integrals over a uniform mesh. Such integrals, due to the presence of the Jastrow factor, converge very rapidly with the number of points in the mesh and thus can be evaluated with a reasonable computational effort.⁵¹

With the aim at reducing the computational cost, calculations are carried out also by replacing the 1s core electrons of oxygen with the pseudopotential approximation, while the hydrogen atoms are treated always with the full Coulomb potential.

The oxygen pseudopotential that we used in both DFT and QMC calculations is the Burkatzki-Filippi-Dolg (BFD) pseudopotential, introduced in Ref. 52. It is built by means of an energy-consistent approach in order to reproduce the valence all-electron excitation energies for a number of different atomic configurations computed at a scalar relativistic Hartree-Fock (HF) level.

Gaussian DFT calculations are performed with a local density approximation (LDA) for the exchange-correlation functional. The optimal basis sets which approach the DFT complete basis set limit are $O(8s8p5d)H(5s3p)$ and $O(9s9p6d)H(5s5p)$ for the pseudopotential and full potential cases, respectively. Ex-

panding the wave function over these basis sets, the variational parameters (α_l, β_l, n_l for each angular momentum l and the one-body Jastrow parameter b) are optimized at the DFT level of theory, by minimizing the total LDA-DFT energy.

B. Variational Quantum Monte Carlo calculations

Quantum Monte Carlo (QMC) refers to several numerical techniques for electronic structure calculations of quantum systems. The interest of the scientific community for these methods has remarkably grown over the last three decades since they were successfully applied to highly correlated electronic systems, and from small- to medium-size quantum chemistry systems.

The QMC techniques used in this work are wave function-based, hence they aim at finding the many-body wave function in a representation as close as possible to the true ground state of the system. The analytic form of the wave function has to be square-integrable and computable in a finite amount of time, but it does not present any further restrictions. This property allows us to introduce correlations in a compact and efficient way.

Another appealing feature of QMC methods is the scaling with the number of particles. Independently of the technique, QMC provides an intrinsic scaling of $\sim N^3$ - N^4 , with N the number of electrons, whereas state-of-the-art coupled cluster single and double (CCSD) is $\propto N^6$ and coupled cluster single, double and triple (CCSD(T)) methods are $\propto N^7$. Therefore QMC approaches allow the treatment of larger molecular clusters with respect to other highly-correlated methods.

Major efforts have been done to reduce the multiplicative scaling prefactor of QMC techniques, i.e. the cost of a single-point calculation. The research has followed two main paths. From one side more compact trial wave functions have been developed. One of the most promising functions is the Jastrow-Antisymmetrized Geminal Power (JAGP) used in this work. A description of the wave function ansatz is given in Subsec. II B 1.

A second way to decrease the scaling prefactor relies on improving the quantum Monte Carlo estimators. QMC total energy calculations are in general much more efficient than those of other observables, due to the *zero-variance* property of the energy estimator. Generally speaking, estimators of other important observables, as the charge density, do not possess this property. Some other bare estimators, as the one for the atomic forces, could have infinite variance. Thus they affect the overall computational efficiency of the QMC calculation. In particular, over the recent years a major improvement has been achieved in the development of an efficient estimator for nuclear forces⁵³⁻⁵⁵.

In the present work, we use a version of this estimator based on the space-warp coordinate transformation⁵⁶ and implemented with an exact infinitesimal differentiation method⁵⁷. This allows a single sample calculation of

the ionic forces with a computational effort of the order of N^3 ; this scaling is comparable to the one for total energy. Moreover, the infinite variance of the space-warped force estimator in the proximity of the nodal surface of the wave function is solved as explained in Refs. 58,63. The latter Reference provides also a nice review on the latest progress in the QMC nuclear forces evaluation. Therefore, by means of this state-of-the-art scheme force estimator we are able to perform efficient structural optimizations at the QMC level of theory also for not-so-light atoms as oxygen.

1. Wave function ansatz

The typical Quantum Monte Carlo wave function is made of a symmetric bosonic factor (*Jastrow factor* applied to an antisymmetric fermionic part (*determinantal part*):

$$\Psi(\mathbf{x}_1, \dots, \mathbf{x}_N) = J(\mathbf{r}_1, \dots, \mathbf{r}_N) \times \psi_D(\mathbf{x}_1, \dots, \mathbf{x}_N), \quad (7)$$

where the set $\{\mathbf{x}_i = (\mathbf{r}_i, \sigma_i)\}$ represents spatial and spin coordinates of the electrons, as in Eq. 3.

The Jastrow factor is a function of the electron-electron separation. It has been proven to be a crucial ingredient in order to well reproduce correlations of the true many-body wave function; it contributes mainly in the description of dynamical correlation effects arising from charge fluctuations. Furthermore, it has been shown⁵⁰ that the Jastrow factor is particularly suitable in the treatment of Van der Waals intermolecular forces. They play an important role also in the physics of the protonated water dimer, therefore an efficient parametrization of the Jastrow is essential.

We split this factor in one-body, two-body and three/four-body terms ($J = J_1 J_2 J_3$).

The one-body factor accounts for electron-ion interactions and it has been already introduced in Eqs. 5,6. The two-body term deals with the electron-electron interactions. In complete analogy with the one-body Jastrow, it is parametrized by a simple function of the electron-electron separation:

$$u(|\mathbf{r}_i - \mathbf{r}_j|) = \frac{1 - e^{-b|\mathbf{r}_i - \mathbf{r}_j|}}{2b}. \quad (8)$$

Then it reads:

$$J_2(\mathbf{r}_1, \dots, \mathbf{r}_N) = \exp\left(\sum_{i < j}^N u(|\mathbf{r}_i - \mathbf{r}_j|)\right). \quad (9)$$

J_1 and J_2 satisfy the Kato cusp conditions⁴⁸, therefore correcting the divergence of the Coulomb potential energy at electron-ion and electron-electron coalescence points, respectively.

The function u rapidly decays to a constant value as the electron-ion and electron-electron distances increase;

thus the large distance behavior of correlations is described by the three/four-body Jastrow term J_3 . It deals with electron-electron-ion (if $a = b$) and electron-ion-electron-ion (in the case $a \neq b$) correlations effects and it represents an essential part of our wave function; therefore we parametrize it in a richer way than the other Jastrow terms:

$$J_3(\mathbf{r}_1, \dots, \mathbf{r}_N) = \exp\left(\sum_{i < j}^N \Phi_J(\mathbf{r}_i, \mathbf{r}_j)\right)$$

$$\Phi_J(\mathbf{r}, \mathbf{r}') = \sum_{a,b}^{N_{\text{atoms}}} \sum_{\mu,\nu}^{N_{\text{Jbasis}}} g_{\mu,\nu}^{a,b} \psi_{a,\mu}^J(\mathbf{r}) \psi_{b,\nu}^J(\mathbf{r}'),$$

where N_{Jbasis} represents the number of GTO's of the primitive Jastrow basis for each atom. The Jastrow uncontracted orbitals $\psi_{a,\mu}^J(\mathbf{r})$ have the same form as the primitive GTO basis set $\psi_{a,\mu}^{\text{GTO}}(\mathbf{r})$ for the determinantal part in Eq. 1. The Jastrow primitive GTO basis used in this work is $[O]3s2p1d[H]2s1p$.

The choice of the fermionic part of the wave function is more delicate. In the case of spin unpolarized systems ($N_\uparrow = N_\downarrow$) of N electrons, we can express it in a general way as an antisymmetrized product of the *geminals* or pairing functions $\Phi(\mathbf{x}_i, \mathbf{x}_j)$ of the system:

$$\Psi_D(\mathbf{x}_1 \dots \mathbf{x}_N) = \hat{A}[\Phi(\mathbf{x}_1, \mathbf{x}_2), \dots, \Phi(\mathbf{x}_{N-1}, \mathbf{x}_N)]$$

$$= \text{pf}(\Phi(\mathbf{x}_i, \mathbf{x}_j)). \quad (10)$$

The geminals are antisymmetric functions of two electron coordinates expressed as a product of a spatial symmetric part and a spin singlet:

$$\Phi(\mathbf{x}_i, \mathbf{x}_j) = \phi(\mathbf{r}_i, \mathbf{r}_j) \frac{\delta(\sigma_i, \uparrow)\delta(\sigma_j, \downarrow) - \delta(\sigma_i, \downarrow)\delta(\sigma_j, \uparrow)}{\sqrt{2}}.$$

The simplest, but computationally most expensive expansion of the geminal is over the *uncontracted atomic orbitals*, and it reads:

$$\phi(\mathbf{r}_i, \mathbf{r}_j) = \sum_{a,b}^{N_{\text{atoms}}} \sum_{\mu,\nu}^{N_{\text{basis}}} \lambda_{\mu,\nu}^{a,b} \psi_{a,\mu}^{\text{GTO}}(\mathbf{r}_i) \psi_{b,\nu}^{\text{GTO}}(\mathbf{r}_j), \quad (11)$$

where the orbitals $\psi_{a,\mu}^{\text{GTO}}(\mathbf{r})$ have the form reported in Eq. 1 with $\mu = (l, m, n)$. N_{basis} represents the number of primitive GTO's per atom. The introduction of the many-body Jastrow factor J in the total QMC wave function (Eq. 7) allows a reduction of the primitive basis set size without loss of accuracy. This reduction has several advantages in the QMC framework. At first it obviously decreases the computational effort for the wave function calculation. Furthermore it also guarantees a more robust energy minimization. Indeed, given the fact that QMC energy derivatives are noisy, using a more compact primitive basis set reduces its redundancy and helps in finding more quickly the global minimum since the number of the effective directions in the Hilbert space

is smaller. The size-reduced primitive basis employed for the determinantal part is $O(5s5p2d)H(4s2p)$ and $O(6s6p2d)H(3s2p)$ for pseudopotential and all-electron calculations, respectively. The number of variational parameters expanded over GTO's atomic orbitals is $P^{\text{AGP}} \propto N_{\text{total basis}} \times (N_{\text{total basis}} + 1)$, where $N_{\text{total basis}}$ is the total number of GTO's in the whole system.

In this work we use two distinct functional forms for ψ_D . They are distinguished by the number of non zero eigenvalues - i.e. the rank - of the matrix $\{\lambda_{\mu,\nu}^{a,b}\}$ in Eq. 11.

The first one is commonly referred as single determinant (SD) and it is recovered when the $\{\lambda_{\mu,\nu}^{a,b}\}$ matrix has the lowest possible rank compatible with the number of electrons in the system, namely when its rank is equal to $N/2$. It can be shown that it is equivalent to the Slater determinant ansatz for HF calculations. In this case the general expansion (11), after diagonalization of the matrix $\{\lambda_{\mu,\nu}^{a,b}\}$, is written as:

$$\phi(\mathbf{r}_i, \mathbf{r}_j) = \sum_k^{N/2} \lambda_k \psi_k^{\text{MO}}(\mathbf{r}_i) \psi_k^{\text{MO}}(\mathbf{r}_j), \quad (12)$$

where $\psi_k^{\text{MO}}(\mathbf{r}) = \sum_{a,\mu} c_{a,\mu}^k \psi_{a,\mu}^{\text{GTO}}(\mathbf{r})$ are *molecular orbitals* (MO). In this work we obtain them starting from the optimized Kohn-Sham orbitals of Gaussian DFT calculations discussed in Sec. II A 2. The number of variational parameters in this case is $P^{\text{SD}} \propto N/2 \times N_{\text{total basis}}$ where $N_{\text{total basis}}$ is the number of linear coefficients for each MO, equal to the total number of GTO's. Close to the CBS limit $N_{\text{total basis}} \gg N$, and so in the SD there is a significant reduction of the number of parameters with respect to the fully uncontracted AGP expansion in Eq. 10. Multiplying the SD by the Jastrow factor one obtains the JSD wave function, which is optimized simultaneously in both the J and SD parts.

The SD represents a particular limit of the function in Eq. 10. Letting the rank of $\{\lambda_{\mu,\nu}^{a,b}\}$ be greater than $N/2$, one introduces multiconfigurational states and goes beyond the single determinant representation. In this more general case the determinantal wave function is called Antisymmetrized Geminal Power (AGP).

The AGP is the particle-conserving version of the Bardeen-Cooper-Schrieffer (BCS) wave function and it accounts for static correlations in the system, namely deriving from nearly-degenerate electronic energy levels. Together with the Jastrow factor it forms the Jastrow-Antisymmetrized Geminal Power (JAGP) wave function which represents a practical implementation of the resonance valence bond idea introduced by Linus Pauling for chemical systems⁵⁹. The JAGP wave function has been proven to be particularly accurate in describing a wide range of strongly correlated systems^{50,60-62}, and it is the second variational form we tested in our work after the JSD.

In order to benefit from the AGP ansatz without paying the cost of dealing with a too large number of variational parameters, which will make the calculation unfeasible for big systems, we develop the AGP expansion on

a contracted basis set. We used atomic hybrid orbitals, also employed in Ref. 63, as contractions of the primitive GTO's. One of the features of the AGP ansatz (without Jastrow) is that the geminal is also the one-body density matrix of the system. With the aim at finding the most effective local (atomic) basis set to describe the whole system, we project the full one-body density matrix on its local atomic constituents, by retaining in the expansion of Eq. 11 only the $\lambda_{\mu,\nu}^{a,b}$'s with $a = b$, and setting to zero the other terms. By diagonalizing the projected one-body density matrix, we obtain a set of local natural orbitals for each atomic fragment. The atomic orbitals obtained in this way are hybrid (i.e. linear combination of primitive Gaussians not restricted to a given angular momentum shell), as they describe the hybridization arising from the atomic embedding, which breaks the spherical symmetry around the nucleus. We call them *atomic hybrid orbitals*. Thanks to this feature, for each atom we keep not only the information on the local electronic structure due to the nuclear charge, but also the information of the nuclear embedding in the compound, namely the impact of the environment on its electronic structure.

The initial AGP useful to fix the hybrid basis can be determined by DFT calculations (in that case the rank of the AGP is $N/2$ as it comes directly from an SD wave function), or by a previously optimized JAGP wave function (in the latter case the Jastrow factor is disregarded and only the determinantal part is taken in the one-body density matrix determination). Once the hybrid basis set is chosen, and the AGP expanded upon it, the geminal reads:

$$\phi(\mathbf{r}_i, \mathbf{r}_j) = \sum_{a,b}^{N_{\text{atoms}}} \sum_{\alpha,\beta}^{N_{\text{hyb}}} \tilde{\lambda}_{\alpha,\beta}^{a,b} \psi_{a,\alpha}^{\text{hyb}}(\mathbf{r}_i) \psi_{b,\beta}^{\text{hyb}}(\mathbf{r}_j), \quad (13)$$

where $\psi_{a,\alpha}^{\text{hyb}}(\mathbf{r}) = \sum_{\mu} c_{\mu}^{\alpha} \psi_{a,\mu}^{\text{GTO}}(r_{ia})$ are the contracted atomic hybrid orbitals, and $\mu = (l, m, n)$ as before. N_{hyb} is the number of atomic hybrid orbitals required for an accurate description of each atom. After their first determination by DFT or by previous JAGP calculations, they are further optimized in the QMC energy minimization.

The number of variational parameters of the wave function is $P^{\text{hyb}} \propto N_{\text{total hyb}}^2 + N_{\text{basis}} \times N_{\text{total hyb}}$, where $N_{\text{total hyb}}$ is the total number of hybrid Gaussians in the whole system. Since $N \approx N_{\text{total hyb}} \ll N_{\text{total basis}}$, the hybrid orbitals represent the optimal basis set, which reduces at most the total number of parameters in the correlated AGP framework. In order to find the best value of N_{hyb} for oxygen and hydrogen, we carried out a detailed analysis of the variational energy versus the hybrid basis size for the single water molecule, reported in Sec. III A.

2. Quantum Monte Carlo methods

All QMC calculations of this work have been carried out with the TURBORVB program⁴³.

All the variational parameters of the JSD and JAGP wave functions have been optimized by means of the stochastic reconfiguration method with Hessian accelerator, also called “linear method”^{50,64–67}. The forces on the parameters and ionic positions have always finite variance thanks to a reweighting scheme for finite systems introduced in Ref. 63 to cure the variance explosion around the nodes of the wave function.

A systematic way of improving the quality of the VMC ansatz is to perform lattice regularized diffusion Monte Carlo (LRDMC) calculations^{68,69}, a projective technique which filters out the high-energy components yielding a more accurate evaluation of the correlation energy. In the case of non-local pseudopotentials, as the one for the oxygen, LRDMC goes beyond the locality approximation, by providing always a variational upper bound of the true ground state energy.

In the present paper, we report on both VMC and LRDMC calculations of the protonated water dimer. The BFD energy-consistent pseudopotential described in Sec. II A 2 has been employed to replace the oxygen-core 1s electrons. Statistical error bars are kept smaller than 0.1 Kcal/mol in all QMC final calculation.

III. RESULTS AND DISCUSSION

We report the results of our QMC study of protonated water dimer. This Section is organized as follows.

The first part (Sec. III A) is devoted to benchmark computations on water molecule which aim at proving the quality of our QMC ansatz.

The second part (Sec. III B) presents the QMC study on the protonated water dimer. Different level of theory are compared with QMC calculations for both geometry and energetics outcomes in order to assess the accuracy of our approach in the study of proton transfer systems.

A. Benchmark calculations of the H_2O molecule

The single water molecule has been the subject of many numerical studies based on several quantum chemistry methods. It is essential to have a good description of its structural and electronic properties in order to tackle the study of larger water clusters, as the intramolecular degrees of freedom will significantly affect the intermolecular environment due to the large water dipole moment and the strong directionality of the H bond.

Here we report our pseudopotential and all-electron calculations on the water molecule with different wave function types and basis sets, with the aim at choosing the best compromise between accuracy and efficiency in order to transfer the most convenient ansatz to the zundel complex and eventually to larger water clusters.

1. Pseudopotential calculations

As reported in Sec. II, the BFD pseudopotential⁵² has been used for oxygen, while the two hydrogens have been treated all-electron. The primitive Gaussian basis set is O(5s,5p,2d) and H(4s,2p) for the determinant, while for the Jastrow factor it is O(3s,2p,1d) and H(2s,1p). Note that the latter basis set has been recently claimed to be one of the most accurate in an extensive QMC study of single molecule water properties⁶³, which used the same Jastrow ansatz as ours. The inhomogeneous three- and four-body Jastrow term (Eq. 10) has been developed directly on the uncontracted primitive basis set, whose flexibility guarantees a very good description of dynamical correlations. On the other hand, for the antisymmetric part we tested two main wave function forms, the single Slater determinant (obtained by using a geminal with rank $N/2$), and the AGP function. The difference in energy between the JSD and the JAGP wave functions, reported in Tab. I, shows the size of static correlations in the system, which amounts to 5-6 mH. This leads also to better geometrical properties, as seen in Tab. III. The JAGP geometry is closer to the experiment than the JSD one, in both the OH distance and the HOH angle. The structural effects of static correlations in the water molecule have been already pointed out in Ref. 63, where they were attributed mainly to a change in the local description of the oxygen atom. In order to analyze in deeper detail the role of the AGP correlations in the water molecule, we studied the natural orbital occupations coming from the diagonalization of the geminal. One of the appealing features of the AGP theory is that the geminal wave function is directly related to the one-body density matrix of the system (without Jastrow factor). Its diagonalization yields the molecular natural orbitals as eigenvectors and their weights are related to the modulus of the AGP eigenvalues which are plotted in Fig. 1. The Figure shows that indeed the orbitals above the HOMO (highest occupied molecular orbital in the single Slater determinant representation) have a sizable weight, with a distribution which falls abruptly to zero only after the 40-th orbital (gray area in the plot). This reflects the multi determinant character of the water molecule, taken into account by the AGP ansatz. We thus believe that, although the entanglement of quantum levels at the origin of static correlations can come from the oxygen atom, its impact in water has a genuine molecular character. Last but not least, the multi determinant AGP representation leads to a better description of the nodal surface of the true ground state, with a gain of about 2.5 mH in the fixed node LRDMC energy with respect to the one obtained by using the JSD as trial wave function, as reported in Tab. IV.

We turn now the attention on how to reduce the AGP basis set in an effective way. So far, both the JSD and JAGP wave functions have been developed on the uncontracted primitive basis in order to exploit at most its flexibility. Thus, the total number of variational param-

TABLE I: Pseudopotential calculations. VMC energies and number of parameters for the QMC wave functions used in this work of the single water molecule, fixed here at the experimental geometry. The BFD pseudopotential has been used for O. The primitive Gaussian basis set is O(5s,5p,2d) and H(4s,2p) for the determinant. The number of total parameters varies depending on the type of contractions used in the determinantal part. The Jastrow functional form has been kept fixed and developed on a primitive Gaussian basis set of O(3s,2p,1d) and H(2s,1p). This gives a number of 213 Jastrow parameters, divided into 184 $g_{\mu,\nu}^{a,b}$, 9 ζ Gaussian exponents in the uncontracted basis, 1 two-body homogeneous Jastrow factor coefficient and 1 parameter for the analogous one-body part. The other parameters come from the determinant, and are reported in the last set of columns.

Wave function ansatz	VMC energies			number of parameters		
	Energy E_x (H)	Variance (H^2)	$E_x - E_{\text{JSD}}$ (mH)	$\lambda_{\alpha,\beta}^{a,b}$	det orbitals	total
JSD (uncontracted orbitals)	-17.24821(7)	0.2655(6)	0.0	682	18	895 ^a
JAGP (hybrid orbitals: 4O 1H)	-17.25013(8)	0.2635(12)	-1.91(11)	21	158	374
JAGP (hybrid orbitals: 4O 5H)	-17.25183(6)	0.2510(6)	-3.62(10)	105	238	538
JAGP (hybrid orbitals: 8O 2H)	-17.25267(7)	0.2426(18)	-4.46(10)	78	298	571
JAGP (hybrid orbitals: 8O 5H)	-17.25302(6)	0.2412(34)	-4.89(10)	171	358	724
JAGP (uncontracted orbitals)	-17.25389(6)	0.2296(5)	-5.68(10)	682	18	895

^aHere the number of parameters is the same as the one in the JAGP wave function since in the JSD ansatz we rewrite the corresponding geminal (of rank $N/2$) on the uncontracted basis in order to optimize the MO's, as explained in Ref. 62.

TABLE II: As Tab. I, but for all-electron calculations. We report here the VMC energies and number of parameters for the all-electron QMC wave functions of the single water molecule, taken at the QMC relaxed geometry. The geometries are reported in Tab. III. The primitive Gaussian basis set is O(6s,6p,2d) and H(4s,2p) for the determinant. The number of total parameters varies depending on the type of contractions used in the determinantal part. The Jastrow functional form has been kept fixed and developed on a primitive Gaussian basis set of O(3s,3p,1d) and H(2s,1p). This gives a number of 418 Jastrow parameters, divided into 406 $g_{\mu,\nu}^{a,b}$, 10 ζ Gaussian exponents in the uncontracted basis, 1 two-body homogeneous Jastrow factor coefficient and 1 parameter for the analogous one-body part. The other parameters come from the determinant, and are reported in the last set of columns.

Wave function ansatz	VMC energies			number of parameters		
	Energy E_x (H)	Variance (H^2)	$E_x - E_{\text{JSD}}$ (mH)	$\lambda_{\alpha,\beta}^{a,b}$	det orbitals	total
JSD (uncontracted orbitals)	-76.40025(8)	1.412(3)	0.0	1383	19	1819
JAGP (hybrid orbitals: 9O 2H)	-76.40504(9)	1.399(6)	-4.79(12)	91	361	870
JAGP (uncontracted orbitals)	-76.40660(7)	1.374(3)	-6.35(11)	1383	19	1819

TABLE III: Geometrical properties of the global minimum of the water molecule. We report a comparison between different QMC wave functions and experimental results⁷⁰.

	\overline{OH} (Å)	$\angle HOH$ (°)
pseudo JSD	0.9542(4)	104.730
pseudo JAGP	0.9549(4)	104.549
all-electron JSD	0.9539(4)	105.187
all-electron JAGP	0.9557(4)	105.101
experiment ⁷⁰	0.95721(30)	104.522(50)

ters is 895 (see the last column of Tab. I), quite large for a single molecule, particularly if one would like to tackle the study of larger water clusters by means of QMC techniques. The most important limitation of this approach is that the number of variational parameters corresponding to the matrix elements $\lambda_{\alpha,\beta}^{a,b}$ increases clearly as the square of the atomic basis size; therefore this should be reduced at minimum in order to make this approach feasible for a large number of molecules.

To this purpose, as explained in Sec. II B 1,

TABLE IV: LRDMC energy results extrapolated to the zero lattice space limit. The LRDMC calculations are performed in the fixed-node approximation. In the last row, we compute the energy gain due to a better nodal description provided by the JAGP wave function with respect to the JSD one. Note that the agreement between the pseudopotential and all-electron calculations has an accuracy of the order of 0.1 mH, despite their very different total energies.

	pseudo	all-electron
E_{JSD} (H)	-17.26280(6)	-76.42475(15)
E_{JAGP} (H)	-17.26528(6)	-76.42690(14)
$E_{\text{JAGP}} - E_{\text{JSD}}$ (mH)	-2.48(9)	-2.15(21)

we define a new smaller basis set by contracting the O(5s,5p,2d)/H(4s,2p) Gaussian primitive basis via atomic natural hybrid orbitals. Each atom in the system is described by its own set of hybrid orbitals. We study how the size of the contracted hybrid basis set affects the quality of the geminal expansion. We compare it with its rigorous lowest energy limit provided by the uncontracted JAGP reference previously computed. The results are re-

ported in Tab. I. The smallest basis set which includes the 1s for H and the 2s and 2p orbitals for O, thus taking into account the 2s2p near degeneracy at the atomic O level, is the 4O 1H hybrid set (in self-explaining notations). It gives the poorest energy and variance among the hybrid basis sets considered, though being lower than the JSD ansatz. The best energy is obtained with the largest hybrid basis tried here, namely the 8O 5H set. It recovers a large fraction of static correlations and its energy is less than 1mH above the uncontracted JAGP one. However, the price to pay is that the parameter reduction is weak, the total number of parameters being close to the one of the full JAGP expansion (see last column of Tab. I). Indeed, while the number of $\lambda_{\alpha,\beta}^{a,b}$ is still significantly lower than the one for the uncontracted basis set, nevertheless the parameters in the contracted orbitals grow too much. The best compromise between efficiency, i.e. total number of variational parameters, and accuracy, i.e. variational energy, is provided by the 8O 2H basis, as it yields a significant gain in energy with a small/moderate number of parameters. This advantage will be remarkable for large number of atoms, as the number of variational parameters corresponding to this atomic natural hybrid orbitals grows only *linearly* with the number of atoms; on the other hand the number of parameters corresponding to $\lambda_{\alpha,\beta}^{a,b}$, grows instead quadratically, but it remains still affordable since it is dramatically reduced by this approach (see Tab. II).

Finally, we study how the AGP spectrum changes with the contracted hybrid basis sets. Fig. 1 shows that, after a complete wave function optimization, the natural orbital eigenvalues magnitude of the hybrid AGP covers the $10^{-2} - 10^{-4}$ range of the fully uncontracted AGP expansion, except for the shortest 4O 1H basis, which clearly spans a too small Hilbert space. Moreover, we checked that the JAGP expanded on the optimal 8O 2H basis gives the same fixed node LRDMC energy as the full JAGP, signalling that the nodal surface is properly described even by the hybrid 8O 2H contraction. Therefore we are going to use it in the study of the protonated water dimer presented after in the paper. As reported in the method Section, the gain in efficiency of the hybrid basis set is expected to be larger and larger as the system size increases, as the quadratic growth of the $\lambda_{\alpha,\beta}^{a,b}$ with the number of atoms depends strongly on the atomic basis size.

2. All-electron calculations

To study the accuracy of the pseudopotential approximation, we carried out also all-electron calculations of the water molecule. With respect to the pseudopotential calculations, the primitive and contracted basis sets for O have been extended in order to account for the additional 1s electrons. The primitive basis set is then O(6s6p2d) and O(3s3p1d) for the determinant and Jastrow term respectively, while the optimal contracted hybrid basis set

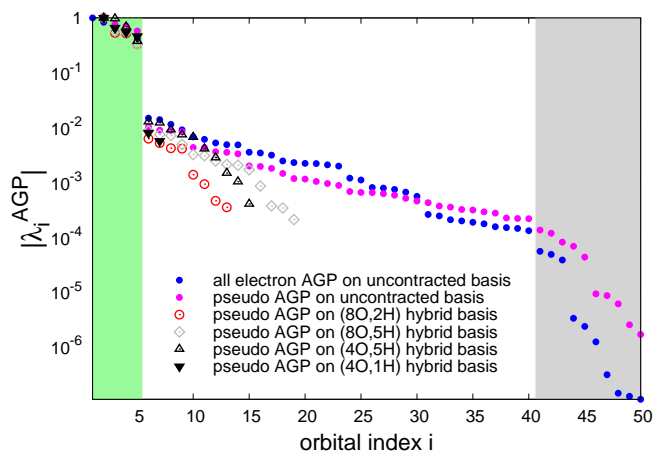


FIG. 1: Semilog plot of the modulus of the AGP eigenvalues versus the molecular orbital index for different basis sets and calculations. The orbital indexes include always the oxygen 1s electrons, replaced in the pseudopotential calculations. The green area represents the exactly occupied molecular orbitals in the single Slater determinant representation, with $\lambda_i = 1$ for $i \in \{1, \dots, \text{HOMO}\}$ and $\lambda_i = 0$ for $i \geq \text{LUMO}$. In the AGP representation, by diagonalizing the geminal we obtain the corresponding molecular orbitals (eigenvectors) and their occupations λ_i^{AGP} (eigenvalues). In the AGP, also the orbitals above the HOMO are occupied, with a weight which jumps across the HOMO to LUMO transition (in going from the green to white region). The gray area shows when the MO occupation tail falls rapidly to zero in the full AGP (expanded on a primitive basis set), signaling that the MO's above that threshold start to be irrelevant to describe the static correlations in the system.

is 9O 2H. In Tab. II we report the variational energies for different wave functions. The energy gain provided by the all-electron JAGP wave function is very close to the one in pseudopotential calculations. The substantial agreement between the two calculations is apparent also in Fig. 1, where the eigenvalues of the higher energy molecular natural orbitals in the AGP behave similarly. The LRDMC energy difference between the JAGP and JSD trial wave functions coincides within the error bars with the one with pseudopotentials. The nodal contribution to the fixed-node energy is the same. The JAGP LRDMC energy is one of the best ever published in literature, in statistical agreement with the one computed by Luchow and Fink⁷¹ (-76.429(1)) H, who used 300 determinants in the trial wave function, and with the one by Zen et al.⁶³ (-76.42660 H), who used the same ansatz as ours in the trial. The JAGP LRDMC projected energy is only 11 mH higher than the extrapolated exact result of 76.438 H⁷².

The all-electron calculations confirm the importance of including static correlations to have a better description of the geometry, as shown in Tab. III. However the HOH angle turns out to be less accurate than the one obtained with pseudopotentials if compared to the experiment, most probably because it is a quantity very

sensitive to the basis set convergence, which is harder to reach in all-electron calculations. Another drawback of all-electron calculations is of course the larger variance for an equivalent wave function ansatz, due to the 1s electron fluctuations, as one can easily evince from the comparison between Tab. I and Tab. II.

Due to the larger primitive basis set required in all-electron calculations, the parameter reduction allowed by the hybrid basis contraction (90 2H) has a great impact on the efficiency. The total number of parameters is reduced by almost a factor of 4 in the determinantal part of the single molecule, without any significant loss of accuracy in the JAGP total energy (see Tab. II).

The use of the BFD pseudopotential for oxygen, and the JAGP ansatz together with the hybrid basis set, tested in the water molecule, is transferred to the protonated water dimer.

B. Protonated water dimer

The protonated water dimer represents the simplest model for proton transfer in aqueous systems. In our work we focus on the energetics of $H_5O_2^+$ related to proton transfer by choosing suitable reaction coordinate (RC). Selecting a RC allows to reduce the complexity of the full-dimensional PES. It projects it onto a single-dimensional subset which retains the most important physical features of the full hypersurface.

Since it is not unique, a correct choice of RC is essential in order to filter out the physical features which suitably describe the considered phenomenon. We propose a mechanism of proton transfer within the dimer which leads to a natural definition of our RC.

As modeled by our system, the proton transfer reaction takes place in three different steps. At first the excess proton is bounded to one water molecule forming an $H_3O^+ + H_2O$ complex. By thermal fluctuations the oxygen-oxygen separation can get closer to the optimal distance of the Zundel complex (around 2.39 Å); at this stage the system assumes a ‘‘Zundel configuration’’ with the proton equally shared between the two oxygens. A further stretch of \overline{OO} disfavors the Zundel configuration and a new $H_2O + H_3O^+$ complex is produced. The overall effect of this process is a transfer of a proton along the hydrogen bond between two oxygen atoms. This mechanism suggests to choose the oxygen-oxygen separation as RC for the dimer potential energy curve.

We present in the following the geometry and energetics of the protonated water dimer. Results on the global minimum geometry are reported at first. The potential energy curve is the result of a stretching of the oxygen-oxygen distance; the behavior of the excess proton is thus investigated along the same path. A particular attention is devoted to the behavior of the $H_3O^+ + H_2O$ complex in the broken-symmetry region of the energy landscape. Proton transfer static barriers at different \overline{OO} distances are calculated in order to further estimate the accuracy of

our approach. All QMC calculations are performed with the JAGP wave function ansatz developed on an atomic hybrid basis set, as discussed in the previous Sec. III A.

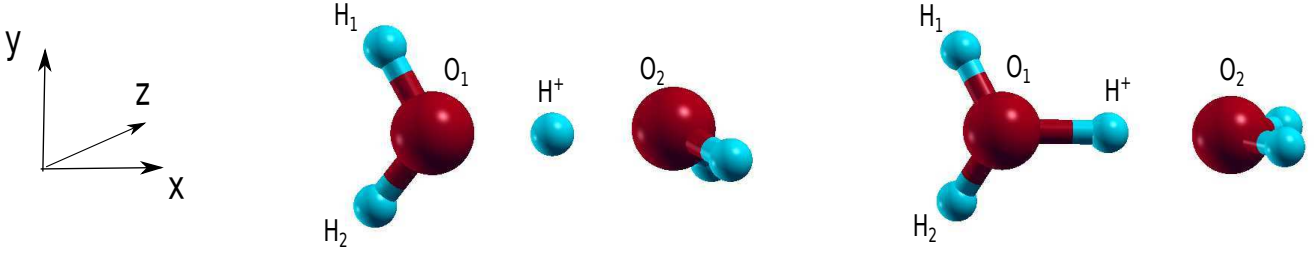
1. Properties of the symmetric global minimum

The minimum energy structure of $H_5O_2^+$ has been debated in the scientific community, as there are two candidates with competing energies: a C_2 -symmetric structure, commonly addressed as Zundel configuration, with the proton evenly shared between the two oxygens, and a C_s -symmetric one with the proton slightly localized on one H_2O molecule (see Fig. 2). Several *ab-initio* investigations^{34,35} have shown that a better treatment of electron correlations turns out in a change of the ground state (GS) geometry from the C_s -sym to the C_2 -sym configuration. Accurate highly-correlated studies^{34,36,37,41} has eventually confirmed that the global minimum is C_2 symmetric.

At a QMC level of theory, the $H_5O_2^+$ GS shows a C_2 Zundel configuration with centrosymmetric excess proton (left part of Figure 2), in agreement with the previous studies. The main geometrical parameters of the global minimum are presented in Tab. V, both for the pseudopotential and all-electron calculations.

If compared with CCSD(T), the QMC ground state geometries show an agreement of up to 0.005 Å in the atomic separations, and up to 1° in the angles. As the angle is close to 180°, in this case its determination is more delicate and could be affected by a larger statistical bias. Therefore we notice a slight discrepancy on this quantity between QMC and coupled cluster outcomes. Nevertheless, these differences do not affect the overall description of the GS and the energetics of the system. In the present work, also the C_s -symmetric structure has been taken into account (left-hand side of Fig. 2). Tab. VI, which reports the VMC optimized C_s geometries, confirms the trend seen in Tab. V for the GS, although the discrepancies in the bond lengths are slightly larger between different methods, the CCSD(T) values being in between the all-electron and pseudopotential VMC results.

The energy difference between the C_s configuration and the C_2 -symmetric global minimum turns out to be 0.25(8) Kcal/mol at VMC level and 0.23(8) Kcal/mol with LRDMC. This is in satisfactory agreement with previous results carried out with Møller-Plesset perturbation theory³⁷ (0.28 Kcal/mol) and CCSD(T)⁴¹ (0.46 Kcal/mol) techniques. The quality of pseudopotential is hence verified also for the Zundel complex. In view of this, its PES along the chosen RC will be worked out mainly with this approximation due to its substantially lower computational demand.

FIG. 2: QMC optimized geometries for global C_2 minimum (left) and for C_s local minimum (right).TABLE V: Geometrical properties (distances in Å, angles in $^\circ$) of the C_2 -symmetry minimum of protonated water dimer, comparison between different computational methods. See Fig. 2 (left-hand side) for atoms notation.

	$\overline{O_1O_2}$	$\overline{O_1H^+}$	$\overline{H^+O_2}$	$\angle O_1H^+O_2$	$\overline{O_1H_1}$	$\overline{O_1H_2}$
DFT-PBE	2.4111	1.2074	1.2074	173.661	0.9697	0.9691
DFT - B3LYP ³⁶			1.2172	173.6	0.9706	0.9701
QMC - with pseudo	2.3847(5)	1.1930(5)	1.1942(8)	174.71(7)	0.9605(8)	0.9650(8)
QMC - all-electron	2.3905(4)	1.1944(6)	1.1989(5)	174.43(9)	0.9630(7)	0.9628(6)
CCSD(T) ⁴¹	2.3864	1.1950	1.1950	173.730	0.9686	0.9682

TABLE VI: Geometrical properties (distances in Å, angles in $^\circ$) of the C_s -symmetry minimum of protonated water dimer. See Fig. 2 (right-hand side) for atoms notation.

	$\overline{O_1O_2}$	$\overline{O_1H^+}$	$\overline{H^+O_2}$	$\angle O_1H^+O_2$	$\overline{O_1H_1}$	$\overline{O_1H_2}$
DFT - B3LYP ³⁶			1.2507	175.4	0.9746	0.9741
QMC - with pseudo	2.3996(6)	1.1154(8)	1.2852(4)	176.5(1)	0.9641(7)	0.9625(4)
QMC - all-electron	2.3913(3)	1.1285(5)	1.2648(4)	175.29(6)	0.9635(4)	0.9616(5)
CCSD(T) ⁴¹	2.3989	1.1233	1.2720	175.646	0.9641	0.9645

2. Stretching the \overline{OO} distance

From the global minimum C_2 -sym configuration we stretch the oxygen-oxygen distance in order to study the potential energy curve and to elucidate the proton transfer properties in the dimer. The structural relaxation at the VMC level for fixed \overline{OO} separation requires a careful procedure due to the flatness of the PES. Starting from a PBE-DFT optimized geometry (see Sec. II A 1 for technical details) and a JAGP variational wave function fully optimized in the electronic part, the atomic coordinates are relaxed with the steepest descent method, considering them as additional variational parameters of the QMC wavefunction.

For the sake of comparison, we minimize a parametrized full-dimensional PES fitted from CCSD(T) calculations⁴¹ to find the best coupled cluster estimates of energy and geometry. By means of the *downhill sim-*

plex minimization technique, we find the configuration of lowest CCSD(T) energy at the same constrained \overline{OO} distance as the corresponding QMC and DFT calculations.

In Fig. 3 we plot the energy landscape along the RC for PBE-DFT, CCSD(T), VMC and LRDMC, the latter computed at the VMC geometry. For VMC technique, we report also full potential calculations for some \overline{OO} separations. We notice a substantial agreement among all techniques in the region at the left of the global minimum of the curve, except for a rigid shift by 0.02 Å between the PBE-DFT results and the others. The PBE \overline{OO} minimum is indeed located at 2.41 Å, while the minimum of the other methods turns out to be at ~ 2.39 Å. Hence this part of the energy curve is only slightly influenced by a better treatment of correlations.

On the other hand, the region at the right of the minimum, at intermediate \overline{OO} distances (≥ 2.55 Å), displays a different behavior. The PBE-DFT overestimates

FIG. 3: Potential energy curve (Kcal/mol) of the protonated water dimer projected on the \overline{OO} distance. Comparison between different computational methods. Structural relaxation is performed at each level of theory. Each curve has its minimum as reference point.

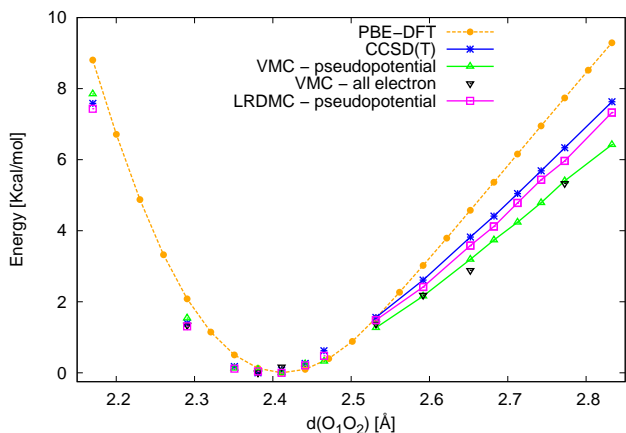
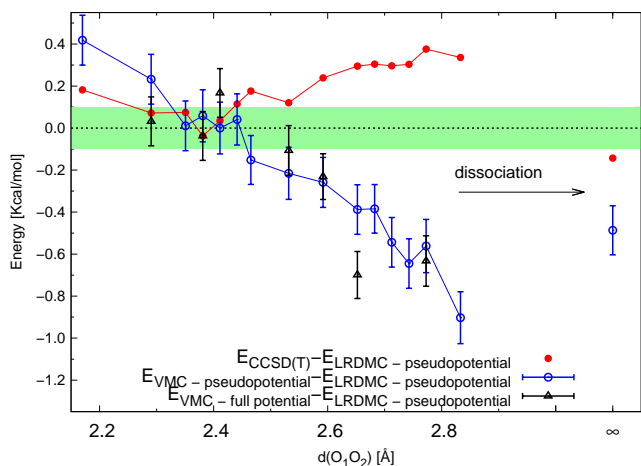


FIG. 4: CCSD(T) and VMC energy landscape (Kcal/mol) as a function of the \overline{OO} distance (\AA) with respect to the LRDMC energies (the zero of the y-axis). Full potential VMC results are reported for few points along with dissociation energies. The green area represents the error bar achieved in typical LRDMC run, i.e. ~ 0.1 Kcal/mol.



the slope of the curve with respect to the most accurate techniques. LRDMC, which yields the best QMC correlation energy, shows a remarkably good agreement with the state-of-the-art CCSD(T) results. In particular all CCSD(T) outcomes are in the range of ≈ 0.3 Kcal/mol, three times the statistical error of the LRDMC calculations, as shown in Fig. 4.

The curves reported in Fig. 3 are obtained with the minimum energy geometry at each level of theory (except for the LRDMC, whose geometry is set at the VMC level). In order to obtain a more reliable comparison and avoid the bias coming from the use of different geome-

FIG. 5: Protonated water dimer energy landscape (Kcal/mol) as a function of \overline{OO} distance (\AA). All the calculations are performed with VMC-optimized geometry. The zero energy reference point corresponds to the minimum of each curve.

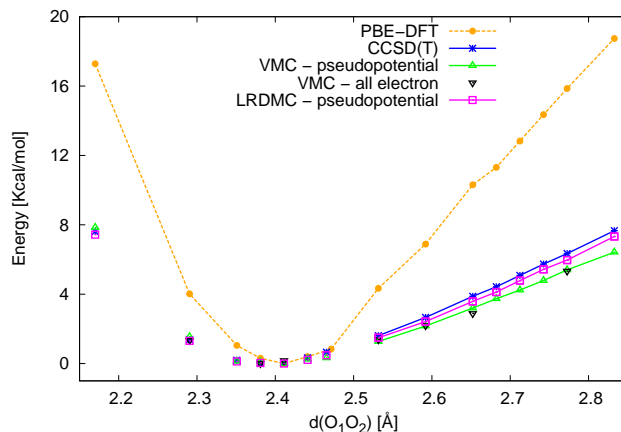
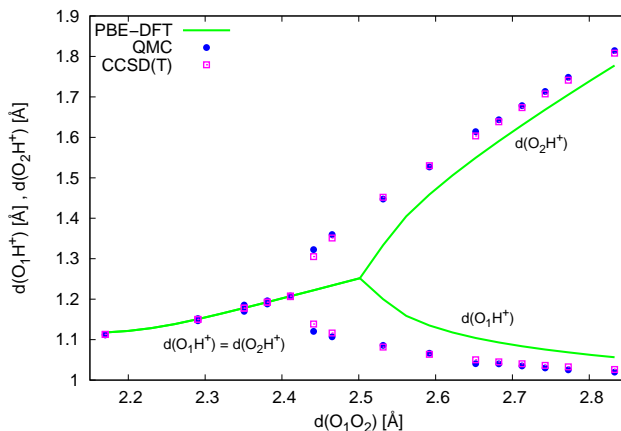


FIG. 6: Separations (\AA) between the two oxygens and the excess proton as a function of the reaction coordinate for different computational methods.



tries, we carried out the same calculations employing the VMC-optimized structures for every technique. The result is reported in Fig. 5. The trend displayed in Fig. 3 for method-optimized geometries is remarkably enhanced when the same configuration of the dimer is considered. Away from the minimum, the PBE-DFT energies show a larger overestimation of the slope.

The slope of the dimer potential energy curve is related to the behavior of the excess proton in the system. In Fig. 6 this property is elucidated. We report in the same plot the separations between the excess proton and each of the two oxygens: $\overline{O_1H^+}$ and $\overline{H^+O_2}$. The structure of the dimer is relaxed at different level of theories with the same procedure carried out for the potential energy curve in Fig. 5. The plot clearly shows the appearance of two distinct regimes of the dimer. One is characterized by a symmetric Zundel configuration with the proton evenly

bonded to the two oxygens; from the point of view of proton transfer physics, it is basically equivalent to the GS configuration. Stretching the \overline{OO} distance results in the formation of a $H_3O^+ + H_2O$ complex with the proton localized on one water molecule. These configurations belong to the *asymmetric regime* of the dimer. Within this regime, the initial C_2 point symmetry of the GS geometry is broken due to proton localization.

Notice that the C_s -sym local minimum presented in Sec. III B 1 displays a localized proton at a distance of ~ 2.39 Å, smaller than the symmetry-breaking distance shown in Fig. 6. However, we verified that if one stretches the \overline{OO} distance starting from this local minimum, the energies obtained are higher than the values plotted in Fig. 3 and Fig. 5.

The distances obtained by the QMC relaxation of the atomic coordinates are in excellent agreement with the CCS(T) calculations; in particular the root mean square distance between the two data sets over the whole \overline{OO} range is of ~ 0.007 Å for both $\overline{O_1H^+}$ and $\overline{O_2H^+}$. Electron correlation plays a key role in determining the stability of the symmetric configuration of the dimer. The overestimation of the potential energy curve slope by PBE-DFT in Fig. 3 corresponds to an overestimation of the symmetry-breaking \overline{OO} separation by ~ 0.13 Å with respect to higher-level post-DFT *ab-initio* methods, and to a very poor description of the geometry in the symmetry-broken region close to the symmetry-breaking point, where the discrepancy in the $\overline{OH^+}$ distances is the largest (going up to 0.15 Å).

3. Implications for more realistic PT models

The zero-temperature potential energy curves reported in Fig. 3 and Fig. 5 seem to conflict with the proton transfer mechanism discussed in the introduction of Sec. III B, since the configuration with centrosymmetric proton is energetically favored and therefore it represents a stable state rather than a transition state between two asymmetric configurations with localized proton.

This contradiction is only apparent. Indeed, Ref. 27 has shown that the introduction of thermal and polarization effects due to the physical environment, favors the asymmetric regime of the complex. Indeed, at finite temperature the *free energy* landscape displays a global minimum shifted towards the asymmetric regime and the Zundel-like structure does not represent anymore the energetically favored configuration. Moreover, a recent experimental result shows that the average \overline{OO} distance in liquid water is of 2.81 Å⁷⁴ which clearly corresponds to a symmetry-broken configuration of the dimer (see Fig. 6). Anyway, in order to jump from a water molecule to one of its neighbors, the proton must pass through a Zundel configuration. Describing correctly the energetics and geometry of the protonated water dimer in the symmetry-breaking transition region is therefore of paramount importance to hope having an accurate description of the

PT in more realistic models.

Indeed, as already mentioned, Fig. 6 highlights that at 0 K a better treatment of electronic correlations turns out in a stability of the asymmetric regime over a considerably wider range of \overline{OO} distances with respect to DFT results. Hence we expect that, at finite temperature and including the surrounding physical environment, the value of the free energy activation barrier for proton transfer would be significantly higher than the PBE-DFT prediction.

4. Properties of the symmetry-broken configurations

In this Section we focus the attention on some relevant properties of the broken-symmetry region where the excess proton is localized on a water molecule. At the QMC level of theory, the formation of a $H_3O^+ + H_2O$ complex occurs at an oxygen-oxygen distance of ~ 2.43 Å in perfect accordance with CCSD(T) results, as seen in Fig. 6.

A quantity which has been extensively studied over the past years^{25,38,76,77} is the *static proton transfer barrier*, i.e. the barrier that the H^+ has to overcome in order to jump from one H_2O molecule to the other at a fixed \overline{OO} distance in the symmetry-broken regime. This quantity does not provide a realistic comparison with the experimental activation barrier for PT, as the \overline{OO} distance will shorten during the proton hopping. Nevertheless, it is relevant in order to provide a further check of the accuracy of our QMC approach. Fixing the \overline{OO} distance, the barriers are obtained as difference between the asymmetric configuration with localized proton and a structure with the excess proton in a centrosymmetric position. Calculations are performed in three representative \overline{OO} separations; the results are shown in Tab. VII where they are compared with existent data in literature.

The first \overline{OO} distance is 2.47 Å, very close to the symmetry-breaking point of the dimer as displayed by highly correlated approaches; on the contrary, at a DFT level the configuration with centrosymmetric proton is still energetically favored, as shown by Fig.6. It has been noticed³⁴ that the PES in this region is particularly flat. Furthermore the potential energy curve of the dimer develops on very tiny energy differences around the symmetry-breaking point. These issues make the calculations in this region of the PES extremely delicate since the stochastic noise can considerably affect the quality of the QMC predictions.

Indeed, Tab. VII shows that QMC and CCSD(T) display a vanishing energy barrier of the order of 0.1 Kcal/mol as the hydrogen is displaced along the oxygen-oxygen axis. The height of this barrier is slightly above the attained statistical error in our typical QMC run. However, despite the very sensitive behavior of the dimer PES around the symmetry-breaking point, the accuracy of our force minimization algorithm allows to account for the tiny energy differences involved; thus it ensures the necessary precision to describe the PT physics in the

dimer. As we discuss in the next Section, a similar accuracy can be achieved in larger molecular clusters with a reasonable amount of computational time. Therefore our QMC framework guarantees a reliable description of the PT physics also for more realistic models.

TABLE VII: Static proton transfer barriers (Kcal/mol) at fixed \overline{OO} separations. Comparison between different level of theory.

Method	$O - O$ distance		
	2.47 Å	2.6 Å	2.7 Å
DFT-PBE	-0.74	0.19	1.94
DFT-PBE (<i>best</i>) ⁷⁷		0.21	1.46
VMC	0.28(6)	2.99(8)	5.99(8)
LRDMC	0.37(8)	2.64(7)	5.57(7)
CCSD(T) - CCSD(T) geometry	0.22	2.37	5.24
CCSD(T) - QMC geometry	0.28	2.29	5.32
CCSD(T) - MP2 geometry ⁷⁷		2.08	4.85
QCISD(T) - MP2 geometry ⁷⁷		2.06	4.82
MS-EVB ²⁵		2.05	5.11
MP2 ⁷⁷		1.77	4.39

The other results are obtained at larger oxygens separations, further from the symmetry-breaking point. They confirm the general behavior already seen along the \overline{OO} RC. LRDMC and CC results are in a good agreement up to 0.2 – 0.3 Kcal/mol, whereas the VMC slightly overestimates the barrier. As well known from previous works, DFT substantially underestimates the barrier with respect to post-DFT methods which provide a better treatment of correlations.

Finally, let us analyze the extreme limit of the asymmetric Zundel configuration, namely when $\overline{OO} \rightarrow \infty$, with the formation of one H₂O and one hydronium. The dissociation energy D_e of $H_5O_2^+$ is computed by setting the distance between the two oxygens to 14 Å. With the CCSD(T) PES, we checked that this is already in the large distance plateau. We get a D_e of 33.02(9) Kcal/mol by VMC, and 32.54(8) Kcal/mol by LRDMC, to be compared with the CCSD(T) value of 32.68 Kcal/mol from Ref. 41, while the PBE-DFT gives $D_e = 29.55$ Kcal/mol. The agreement between the LRDMC and CCSD(T) is impressive, while it is already good for the VMC estimate. This is mainly due to the size consistency of the JAGP ansatz, obtained once the Jastrow is close to the complete basis set limit. The VMC and CCSD(T) dissociation energies are plotted in Fig. 4 with respect to LRDMC values.

5. Test on a larger molecular cluster

QMC methods present a favorable scalability with the number of particles with respect to other highly correlated approaches such as CC. With the aim at proving this feature also for our approach, we performed a benchmark calculation on a more realistic PT model composed

TABLE VIII: Total computational wall time in hours of typical VMC and LRDMC runs, performed with the program TurboRVB⁴³ on 512 thin nodes of the Curie HPC machine (2.7 GHz 8 core Intel Sandy Bridge processors), to reach a target statistical error of 0.06 Kcal/mol in total energies. Single water molecule, protonated dimer and a larger cluster of 6 water molecule and one excess proton are compared. The LRDMC is carried out at a lattice space of $0.125 a_0$.

# of water molecules	Total wall time (h) on 512 CPU	
	VMC	LRDMC
1	0.05	0.15
2	0.24	2.13
6	6.49	164.35

of 6 water molecules and one excess proton, which will be the subject of a further study. In Table VIII we report a comparison of the computational time required to carry out typical VMC and LRDMC runs for different sizes of the protonated water cluster at fixed optimized variational parameters and geometry. The calculations have been carried out on the HPC Curie thin nodes (2.7 GHz 8 core Intel Sandy Bridge processors), and performed with a target statistical error of 0.06 Kcal/mol in the total energy. By performing a simple fit on the data in Table VIII, we notice that the simple VMC displays a $\sim N^3$ scaling with the number of particles; the more accurate LRDMC, carried out at a lattice space of $a = 0.125a_0$, shows instead an almost perfect N^4 scaling. However, the LRDMC calculations are still feasible in a reasonable computational time for the 6 H₂O cluster, while the VMC is still cheap at that cluster size.

IV. CONCLUSIONS

In this paper we presented an extensive study of the protonated water dimer by means of the VMC and LRDMC techniques.

The JAGP ansatz employed in this work implements an accurate treatment of both static and dynamical correlations among electrons. The expansion of the determinantal part over atomic hybrid orbitals ensures a drastic reduction of the number of variational parameters thus making the wave function optimization procedure efficient and robust even for large systems. The comparison with previous published QMC calculations on the single water molecule showed the quality of our wave function ansatz.

Total energy calculations are performed with the less expensive Variational Monte Carlo approach along with the more precise projective Diffusion Monte Carlo. The powerful minimization algorithm implemented in our QMC software, allows an efficient estimation of the forces acting on each atomic component with a reasonable computational cost. Hence both energetics and geometry calculations are performed within the QMC framework.

A simple mechanism of proton transfer in the dimer has been presented and exploited to choose a suitable reaction coordinate for the potential energy curve. The energy landscape as a function of the oxygen-oxygen distance is computed and compared with density functional theory in the PBE approximation and with CCSD(T) results; LRDMC is in excellent agreement with CCSD(T) calculations (within 0.2 – 0.3 kcal/mol), whereas minor differences (up to about 1 kcal/mol) are shown by VMC. Ref. 79 has recently reported a similar accuracy for small water clusters by diffusion Monte Carlo calculations.

Geometrical properties of the excess proton are also investigated by VMC structural relaxations, which provide geometries remarkably close to the ones obtained by a CCSD(T) fitted PES. We show the presence of two distinct regimes of the dimer depending on the oxygen-oxygen distance: one with a centrosymmetric excess proton and the other with the proton localized on one of the water molecules. The stability of these configurations crucially depends on the level of theory employed to describe the electronic structure of the system. A better treatment of electron correlation results in the stability of the asymmetric proton geometry over a wider range of OO distances.

These results, together with the proton transfer static barrier and the dissociation energy D_e , show that our QMC approach has a global accuracy comparable with the state-of-the-art coupled cluster in both geometry and

energetics of the dimer, with the advantage of having a better scaling with the number of particles.

The accuracy shown by our QMC calculations combines with a favorable scalability with the number of particles with the respect to other highly correlated techniques, as demonstrated with a test simulation on a larger protonated water cluster.

These features make this approach a very promising candidate for the study of proton transfer in complex aqueous systems. In particular, we have shown that the VMC method is cheap, provides very accurate geometries and a global accuracy of less than 1 kcal/mol in the most important region for the PT physics. We hope that our work will inspire further studies on this direction, and pave the way for accurate highly-correlated simulations of more realistic proton transfer models which will eventually shed new insights onto the PT mechanism in water.

Acknowledgments

We thank Joel M. Bownman and Xinchuan Huang who provided us the coupled cluster potential energy surface of $H_5O_2^+$. One of us (Michele Casula) acknowledges computational resources in the form of the GENCI grant number x2013096493.

* Electronic address: mario.dagrada@impmc.upmc.fr

† Electronic address: michele.casula@impmc.upmc.fr

‡ Electronic address: marco.saitta@impmc.jussieu.fr

§ Electronic address: sorella@sissa.it

¶ Electronic address: francesco.mauri@impmc.jussieu.fr

¹ W. L. Jorgensen, J. Chandrasekhar, J. D. Madura, R. W. Impey, M. L. Klein, *J. Chem. Phys.* **79**, 926 (1983).

² M. Sprik, *J. Phys. Chem.* **95**, 2283 (1991).

³ M. W. Mahoney, W. L. Jorgensen, *J. Chem. Phys.* **112**, 8910 (2000).

⁴ P. L. Silvestrelli, M. Parrinello, *J. Chem. Phys.* **111**, 3572 (1999).

⁵ J. C. Grossman, E. Schwegler, E. W. Draeger, F. Gygi, G. Galli, *J. Chem. Phys.* **120**, 300 (2004).

⁶ J. VandeVondele, F. M. and M. Krack, J. Hutter, M. Sprik, M. Parrinello, *J. Chem. Phys.* **122**, 014515 (2005).

⁷ R. Jonchiere, A. P. Seitsonen, G. Ferlat, A. M. Saitta, R. Vuilleumier, *J. Chem. Phys.* **135**, 154503 (2011).

⁸ R. Z. Khaliullin, T. D. Kühne, arXiv/1303.2067 (2013).

⁹ P. Carloni, U. Rothlisberger, M. Parrinello, *Acc. Chem. Res.* **35**, 455 (2002).

¹⁰ R. A. Friesner, B. D. Dunietz, *Acc. Chem. Res.* **34**, 351 (2001).

¹¹ S. Yoo, X. C. Zeng, S. S. Xantheas, *J. Chem. Phys.* **130**, 221102 (2009).

¹² H. S. Lee, M. E. Tuckerman, *J. Chem. Phys.* **126**, 164501 (2007).

¹³ C. J. D. von Grothuss, *Ann. Chim.* **LVIII**, p. 54 (1806).

¹⁴ N. Agmon, *Chem. Phys. Lett.* **244**, 456 (1995).

¹⁵ D. Marx, *ChemPhysChem*, **7**, 1848 (2006).

¹⁶ T. E. Decoursey, *Physiol Rev.* **83**, 475 (2003).

¹⁷ E. Freiera, S. Wolfb, K. Gerwerta, *Proc. Natl. Acad. Sci.* **108**, 11435 (2011).

¹⁸ J. Deisenhofer, O. Epp, I. Sinning, H. Michel, *J. Mol. Biol.* **246**, 429 (1995).

¹⁹ D. Lancaster, H. Michel, B. Honig, M. Gunner, *Biophys. J.* **70**, 2469 (1996).

²⁰ M. Eigen, *Angew. Chem. Int. Ed.* **3**, 1 (1964).

²¹ O. F. Mohammed, D. Pines, J. Dreyer, E. Pines, E. T. J. Nibbering, *Science* **310**, 83 (2005).

²² O. F. Mohammed, D. Pines, E. Pines, E. T. J. Nibbering, *Chem. Phys.* **341**, 240 (2007).

²³ Z. Luz, S. Meiboom, *J. Am. Chem. Soc.* **86**, 4768 (1964).

²⁴ Noam Agmon, *Hydrogen bonds, water rotation and proton mobility.*, *J. Chim. Phys. (Paris)*, **93**, 1714 (1996).

²⁵ U. W. Schmitt, G. A. Voth, *J. Chem. Phys.* **111**, 9361 (1999).

²⁶ H. Lapid, N. Agmon, M. K. Petersen, G. A. Voth, *J. Chem. Phys.* **122**, 014506 (2005).

²⁷ D. Marx, M. E. Tuckerman, J. Hutter, M. Parrinello, *Nature* **397**, 601 (1999).

²⁸ O. Markovitch, H. Chen, S. Izvekov, F. Paesani, G. A. Voth, N. Agmon, *J. Phys. Chem. B* **112**, 9456 (2008).

²⁹ D. Marx, A. Chandra, M. E. Tuckerman, *Chem. Rev.* **110**, 21742216 (2010).

³⁰ A. M. Saitta, F. Saija, P. V. Giaquinta, *Phys. Rev. Lett.* **108**, 207801 (2012)

³¹ A. Hassanali, F. Giberti, J. Cuny, T. D. Kühne, M. Par-

- rinello, Proc. Natl. Acad. Sci. USA **110**, 13723 (2013).
- ³² E. Wicke, M. Eigen, H. Ackermann, Z. Phys. Chem. (N.F.) **1**, 340 (1954).
- ³³ G. Zundel, H. Metzger, Z. Phys. Chem **58**, 225 (1968).
- ³⁴ Y. Xie, R. B. Remington, H. F. Schaefer, J. Chem. Phys. **101**, 4878-4884 (1994).
- ³⁵ E. F. Valeev, H. F. Schaefer, J. Chem. Phys. **108**, 7197-7201 (1998).
- ³⁶ D. J. Wales, J. Chem. Phys. **110**, 10403 (1999).
- ³⁷ A. A. Auer, T. Helgaker, and W. Klopper, Phys. Chem. Chem. Phys. **2**, 2235 (2000).
- ³⁸ D. Wei, D. R. Salahub, J. Chem. Phys. **101**, 7633 (1994).
- ³⁹ M. E. Tuckerman, D. Marx, M. L. Klein, M. Parrinello, Science **275**, 817 (1997).
- ⁴⁰ J. M. Headrick, E. G. Diken, R. S. Walters, N. I. Hammer, R. A. Christie, J. Cui, E. M. Myshakin, M. A. Duncan, M. A. Johnson, K. D. Jordan, Science **308**, 1765 (2005).
- ⁴¹ X. Huang, B. J. Braams, J. M. Bowman, J. Chem. Phys. **122**, 044308 (2005).
- ⁴² P. Giannozzi *et al.*, J. Phys.: Condens. Matter **21**, 395502 (2009).
- ⁴³ <http://people.sissa.it/~sorella/web/>
- ⁴⁴ J. P. Perdew, K. Burke, and M. Ernzerhof, Phys. Rev. Lett., **78**, 1396 (1997).
- ⁴⁵ T. D. Kühne, M. Krack, M. Parrinello, J. Chem. Theory Comput. **5**, 235 (2009)
- ⁴⁶ Trouiller N., Martins J., Phys. Rev. B, **43**, 1993 (1991).
- ⁴⁷ R. Car, M. Parrinello, Phys. Rev. Lett. **55**, 2471 (1985).
- ⁴⁸ T. Kato, Comm. Pure Appl. Math. **10**, 151 (1957).
- ⁴⁹ M. Holzmann, D. M. Ceperley, C. Pierleoni, and K. Esler Phys. Rev. E **68**, 046707 (2003).
- ⁵⁰ S. Sorella, M. Casula, D. Rocca, J. Chem. Phys. **127**, 014105 (2007).
- ⁵¹ S. Azadi, C. Cavazzoni, S. Sorella, Phys. Rev. B **82**, 125112 (2010)
- ⁵² M. Burkatzki, C. Filippi, M. Dolg, J. Chem. Phys. **126**, 234105 (2007).
- ⁵³ R. Assaraf and M. Caffarel, J. Chem. Phys. **119**, 10536 (2003).
- ⁵⁴ S. Chiesa, D. Ceperley, S. Zhang, Phys. Rev. Lett. **94**, 036404 (2005).
- ⁵⁵ A. Badinski, P. D. Haynes, J. R. Trail, R. J. Needs, J. Phys.: Condens. Matter **22**, 074202 (2010).
- ⁵⁶ C. Filippi, C. J. Umrigar, Phys. Rev. B **61**, 16291 (2000).
- ⁵⁷ S. Sorella, L. Capriotti, J. Chem. Phys. **133**, 234111 (2010).
- ⁵⁸ C. Attaccalite and S. Sorella, Phys. Rev. Lett. **100**, 114501 (2008).
- ⁵⁹ L. Pauling, *The nature of the chemical bond*, 3rd edition, Cornell University Press, Ithaca, New York.
- ⁶⁰ D. Nissenbaum, L. Spanu, C. Attaccalite, B. Barbiellini, A. Bansil, Phys. Rev. B **79**, 035416 (2009).
- ⁶¹ F. Sterpone, L. Spanu, L. Ferraro, S. Sorella, L. Guidoni, J. Chem. Theory Comput., **4**, 1428 (2008).
- ⁶² M. Marchi, S. Azadi, M. Casula, S. Sorella, J. Chem. Phys. **131**, 154116 (2009).
- ⁶³ A. Zen, Y. Luo, S. Sorella, L. Guidoni, J. Chem. Theory Comput. **9**, 4332 (2013).
- ⁶⁴ S. Sorella, L. Capriotti, Phys. Rev. B, **61**, 2599 (2000).
- ⁶⁵ S. Sorella, Phys. Rev. B, **64**, 024512 (2001).
- ⁶⁶ S. Sorella, Phys. Rev. B, **71**, 241103 (2005).
- ⁶⁷ C. J. Umrigar, J. Toulouse, C. Filippi, S. Sorella, R. G. Hennig, Phys. Rev. Lett. **98**, 110201 (2007).
- ⁶⁸ M. Casula, C. Filippi, S. Sorella, Phys. Rev. Lett. **95**, 100201 (2005).
- ⁶⁹ M. Casula, S. Moroni, S. Sorella, C. Filippi, J. Chem. Phys. **132**, 154113 (2010).
- ⁷⁰ W. S. Benedict, N. Gailar, E. K. Plyler, J. Chem. Phys. **24**, 1139 (1956).
- ⁷¹ A. Lüchow and R. Fink, J. Chem. Phys. **113**, 8457 (2000).
- ⁷² D. Feller, C. Boyle, and E. Davidson, J. Chem. Phys. **86**, 3424 (1987).
- ⁷³ M. Park, I. Shin, N. J. Singh, K. S. Kim, J. Phys. Chem. A, **111**, 10692-10702 (2007).
- ⁷⁴ U. Bergmann, A. Di Cicco, P. Wernet, E. Principi, P. Glatzel *et al.*, J. Chem. Phys. **127**, 174504 (2007).
- ⁷⁵ S. S. Xantheas, J. Am. Chem. Soc. **117**, 10373 (1995).
- ⁷⁶ M. Pavese, S. Chawla, D. Lu, J. Lobaugh, G.A. Voth, J. Chem. Phys. **107**, 7428 (1997).
- ⁷⁷ S. Sadhukhan, D. Munoz, C. Adamo, G. E. Scuseria, Chem. Phys. Lett **306**, 83-87 (1999).
- ⁷⁸ E. Neuscamman, Phys. Rev. Lett. **109**, 203001 (2012)
- ⁷⁹ M. J. Gillan, F. R. Manby, M. D. Towler, D. Alfè, J. Chem. Phys. **136**, 244105 (2012)